Stars and their variability observed from space
C. Neiner, W. W. Weiss, D. Baade, R. E. Griffin, C. C. Lovekin, A. F. J. Moffat (eds)

A NOVEL MODELING OF MAGNETO-ROTATING STELLAR EVOLUTION

K. Takahashi[1]

Abstract. About 10% of massive and intermediate-mass main-sequence stars possess strong surface magnetic fields, and the magnetic massive stars may be progenitors of strongly magnetized neutron stars known as magnetars. However, the evolution of magnetic fields in stellar interiors remains a big open question for stellar evolution theory. We have developed a new stellar evolution code that is capable to follow a long-timescale evolution of stellar magnetism. First, the structure of the stellar field is significantly simplified to have axially symmetric toroidal + poloidal components. Then the evolution of the two-component magnetic field is described by the mean-field dynamo equation. The new formalism self-consistently includes the effects of the Ω-dynamo, which results from large scale shear in the rotation flow, magnetic dissipation, and angular momentum transfer due to magnetic stress. We will present our preliminary results and discuss how the model can be verified by observations.

Keywords: Stars: evolution — Stars: magnetic field — Stars: rotation

1 Introduction

Magnetic stars account for about ∼10% of radiative main sequence stars of OBA types (Landstreet 1992). Their strong (typically ∼100-1000 G) fields are characterized by a large-scale (∼dipole) structure and long-timescale (∼10 yr) stability (Wade et al. 2000; Silvester et al. 2014). No correlations between the field strength and fundamental parameters have been found so far. These properties would be compatible with a fossil field, i.e., a remnant of star formation that survives in a stable configuration (Braithwaite & Spruit 2017).

The evolution of radiative main sequence stars, which are the progenitors of magnetic white dwarfs and neutron stars, can be significantly affected by strong magnetic fields. Because of the intrinsically strong stellar wind, the magnetic breaking for massive OB type stars can be significant enough to be observed (e.g., σ-Ori E; Townsend et al. 2010). Strong surface fields can even trap the wind material into a corotating magnetosphere, which provides substantial understanding for X-ray emission of IQ Aur (Babel & Montmerle 1997) or phase variations of Balmer-line emissions of σ-Ori E (Townsend & Owocki 2005). Besides, strong magnetic stress that is furnished by the internal field may account for the efficient angular momentum transfer in a radiatively stratified region (Spruit 1999).

The purpose of this work is to present a new framework of stellar evolution modeling, in which the evolution of stellar magnetic fields and rotation is treated in a physically consistent manner. The axisymmetric dipole approximation is applied to the magnetic field structure. The field evolution equation is formulated starting from the mean-field MHD equation. We utilize a path integral for the averaging, which yields the conservation law of magnetic flux in the case of no dissipation. Also, the angular momentum transfer due to the Lorentz force is expressed by defining the Maxwell stress tensor, which naturally yields a conservative expression for the magnetic angular momentum transfer.

In this proceedings, simulation results of the code test as well as the magneto-rotating stellar evolution of intermediate-mass radiative stars are presented. The detailed information will be reported in Takahashi & Langer (2019).

2 Field evolution coupled with stellar rotation

2.1 Magnetic flux conservation

We have calculated a 1.5 $M_\odot$ stellar evolution with a magnetic field but switching off the magnetic dissipation and the Ω-effect. The evolution is followed from the zero age main sequence (ZAMS) phase until the star starts core helium burning and enters into the red clump in the Hertzsprung-Russell Diagram.

[1] Max-Planck-Institut für Gravitationsphysik / Albert-Einstein-Institut, Am Mülenberg 1, 14476 Potsdam-Golm, Germany

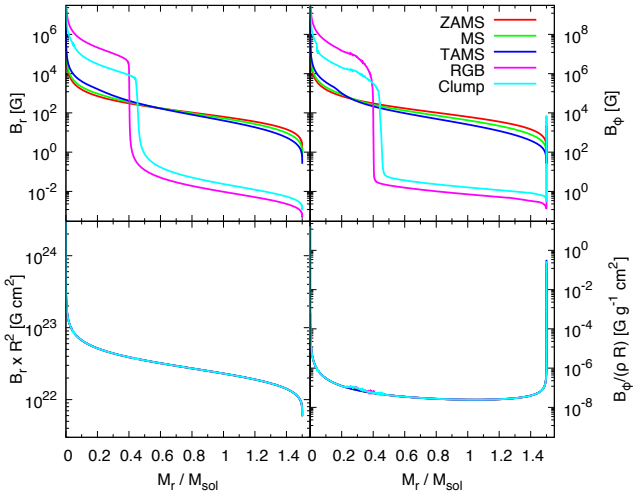

Fig. 1. Evolution of the internal magnetic fields at the ZAMS (red), at the middle of the main sequence phase (MS; green), at TAMS (blue), at the middle of the red giant phase (RG; magenta), and at the red clump phase (Clump; cyan). The top two panels show the evolution of the radial component (B_r; left) and the toroidal component (B_ϕ; right). The bottom two panels show the evolution of conserved quantities, $B_r r^2$ at the left and $B_\phi/\rho r$ at the right.

Figure 1 shows the resulting evolution of the internal magnetic field. The top two panels, which show radial and toroidal magnetic field components, exhibit the effect of contraction and expansion during stellar evolution. They show that the magnetic field in the central core of $<\sim 0.4$ M$_\odot$ is amplified by about two orders of magnitude, while that in the outer envelope is reduced by about four orders of magnitude. Nevertheless, the two quantities which are shown in the bottom panels, are entirely conserved during the whole evolutionary phases. Only a small fluctuating deviation is seen for $B_\phi/\rho r$ at $\sim$0.3–0.4 M$_\odot$. This results from automated mesh refinement, which is done to capture the thin structure of the hydrogen-burning shell that surrounds the helium core.

2.2 Torsional wave solution

Differential rotation winds up the poloidal magnetic field to produce a toroidal component. As the toroidal component gets strong, the magnetic stress increases as well, counteracting to reduce the differential rotation. We have found that the basic equations that describe the evolution of the toroidal field component and the angular momentum can be approximated by a set of hyperbolic differential equations. Therefore, we can expect that a wave that propagates with the speed of about the Alfvén velocity is formed in this system.

Taking the 1.5 M$_\odot$ main-sequence stellar structure as the background, which has a radius of $\sim$ 1.5 R$_\odot$, we have calculated the coupled evolution of the toroidal field and the rotation frequency, taking the Ω-effect and the magnetic stress into account, but turning the viscosity and the magnetic diffusivity off. A uniform $B_r = 500$ G is applied. A step-function distribution of $\Omega = 10^{-4}$ rad s^{-1} for $M \leq 1$ M$_\odot$, or $\Omega = -10^{-4}$ rad s^{-1} otherwise, is applied for the initial Ω distribution. B_ϕ is set uniformly to be zero.

Figure 2 shows the result. As we have expected, the formation and propagation of torsional waves are well captured by the simulation. The wave velocity becomes $c \sim 80$ cm s^{-1}, and correspondingly, the wave-crossing time from the center to the surface becomes $\sim 1.3 \times 10^9$ s $\sim$ 41 yr. We have noticed that the torsional wave results in two important outcomes. The first is that the wave accounts for the significantly efficient angular momentum transport. When the dissipations in both mechanical and magnetic components are switched on, the wave propagates through the stellar interior while it dissipates to distribute the angular momentum to other regions. The model finally reaches rigid rotation. The second outcome is that the star starts to oscillate torsionally during the transitional period towards rigid rotation. The oscillation frequency is comparable to the wave-crossing time. This torsional oscillation may be compatible with the period change of stellar rotation observed in several B-type stars (Krtička et al. 2017; Shultz et al. 2018, 2019).

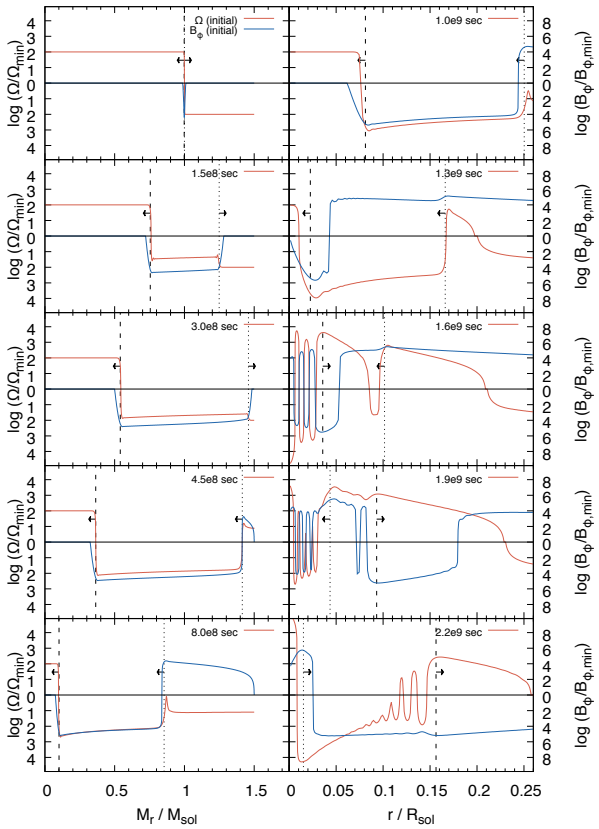

Fig. 2. Wave propagation illustrated by 10 different time snapshots. The logarithm of Ω or B_ϕ is shown by either a red or a blue line. The horizontal axis for the left panels, in which waves before 8×10^8 s are shown, is the enclosed mass. For the right panels, in which waves after 1×10^9 s are shown, the radius is taken as the horizontal axis. The black dashed and black dotted lines show the estimated positions of the wave fronts, and arrows indicate directions of the propagation. Critical values of $\Omega_{\rm min} = 1 \times 10^{-6}$ rad s^{-1} and $B_{\phi,{\rm min}} = 1 \times 10^3$ G are used.

3 Evolution toward a red giant

As a demonstration of the capability of our method, we have calculated the stellar evolution up to the central helium ignition of a solar metallicity 1.5 $M_\odot$ magneto-rotating star. For the initial distributions of rotation and magnetic field, rigid rotation with $\Omega = 5.0 \times 10^{-5}$ rad s^{-1} (equivalent to $P_{\rm rot} = 1.4$ d), zero toroidal field component of $B_\phi = 0$, and a uniform radial component of $B_r = 10$ G are applied. In this calculation, we test two types of angular velocity profiles in a convective region. The first one is the rigid rotation, $\Omega(r) \sim r^0$, and the other is $\Omega(r) \sim r^{-1}$.

Evolution of the surface and core rotation periods are shown in Fig. 3. The core spin period of the Ω-constant model, which is shown by the red solid line, agrees with the surface periods shown by the black dashed line up to the point of $\log R/R_\odot = 1.7$. Meanwhile, not only the core rotation period but also the surface period of the $\Omega \sim r^{-1}$ model simultaneously explain the observations.

4 Conclusions

We have developed a new framework to follow the evolution of magneto-rotating stars. The time-dependent and global basic equations have the torsional wave solution. We predict that a magnetic star can oscillate torsionally, which may be compatible with the observed rotational period change. Moreover, the dissipating wave can account for the efficient angular momentum transport inside the star. We plan to apply this new formulation to general purpose stellar evolution simulations in the future.

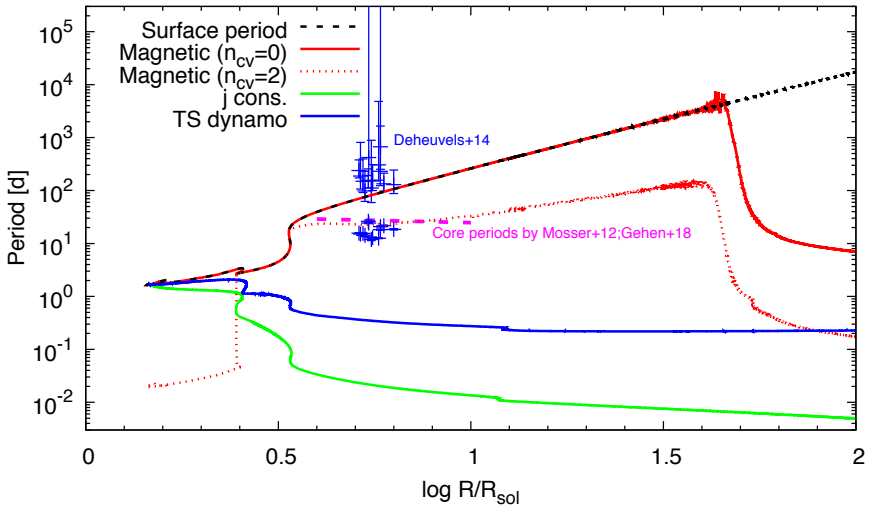

Fig. 3. Period evolution of the 1.5 $M_\odot$ stellar models. Surface and core rotation periods of the $\Omega \sim r^0$ model are shown by black dashed and red solid lines, and the core rotation period of the $\Omega \sim r^{-1}$ model is shown by the red dotted line. Core periods of models with no angular momentum transfer and with transfer due to the Tayler-Spruit dynamo are shown by green and blue solid lines. Theoretical models are compared with the observations of the core rotation periods by Mosser et al. (2012); Gehan et al. (2018) (purple dashed line) and of both the surface and the core periods by Deheuvels et al. (2014) (blue pluses).

References

Babel, J. & Montmerle, T. 1997, A&A, 323, 121
Braithwaite, J. & Spruit, H. C. 2017, Royal Society Open Science, 4, 160271
Deheuvels, S., Doğan, G., Goupil, M. J., et al. 2014, A&A, 564, A27
Gehan, C., Mosser, B., Michel, E., Samadi, R., & Kallinger, T. 2018, A&A, 616, A24
Krtička, J., Mikulášek, Z., Henry, G. W., Kurfürst, P., & Karlický, M. 2017, MNRAS, 464, 933
Landstreet, J. D. 1992, A&A Rev., 4, 35
Mosser, B., Goupil, M. J., Belkacem, K., et al. 2012, A&A, 548, A10
Shultz, M., Rivinius, T., Das, B., Wade, G. A., & Chand ra, P. 2019, MNRAS, 486, 5558
Shultz, M. E., Wade, G. A., Rivinius, T., et al. 2018, MNRAS, 475, 5144
Silvester, J., Kochukhov, O., & Wade, G. A. 2014, MNRAS, 440, 182
Spruit, H. C. 1999, A&A, 349, 189
Takahashi, K. & Langer, N. 2019, in prep.
Townsend, R. H. D., Oksala, M. E., Cohen, D. H., Owocki, S. P., & ud-Doula, A. 2010, ApJ, 714, L318
Townsend, R. H. D. & Owocki, S. P. 2005, MNRAS, 357, 251
Wade, G. A., Donati, J. F., Landstreet, J. D., & Shorlin, S. L. S. 2000, MNRAS, 313, 851